Geophysical Journal International

Geophys. J. Int. (2020) **221,** 1232–1247
Advance Access publication 2020 February 14
GJI Seismology

doi: 10.1093/gji/ggaa076

Crustal structure of the Azores Archipelago from Rayleigh wave ellipticity data

Ana M. G. Ferreira,[1,2] Augustin Marignier,[2,3] Januka Attanayake,[4] Michael Frietsch[2] and Andrea Berbellini[5]

[1]*CERIS, Instituto Superior Técnico, Universidade de Lisboa, Av. Rovisco Pais* 1, 1049-001 *Lisboa, Portugal. E-mail: a.ferreira@ucl.ac.uk*
[2]*Department of Earth Sciences, Faculty of Mathematical & Physical Sciences, University College London, WC*1*E* 6*BT, United Kingdom*
[3]*Mullard Space Science Laboratory, University College London, RH*56*NT, United Kingdom*
[4]*School of Earth Sciences, University of Melbourne, Parkville, VIC* 3010*, Australia*
[5]*Istituto Nazionale di Geofisica e Vulcanologia, Sezione di Bologna, Via Donato Creti* 12*,* 40128 *Bologna, Italy*

Accepted 2020 February 3. Received 2019 December 26; in original form 2019 September 12

SUMMARY

Determining the crustal structure of ocean island volcanoes is important to understand the formation and tectonic evolution of the oceanic lithosphere and tectonic swells in marine settings, and to assess seismic hazard in the islands. The Azores Archipelago is located near a triple junction system and is possibly under the influence of a mantle plume, being at the locus of a wide range of geodynamic processes. However, its crustal structure is still poorly constrained and debated due to the limited seismic coverage of the region and the peculiar linear geometry of the islands. To address these limitations, in this study we invert teleseismic Rayleigh wave ellipticity measurements for 1-D shear wave speed (V_S) crustal models of the Azores Archipelago. Moreover, we test the reliability of these new models by using them in independent moment tensor inversions of local seismic data and demonstrate that our models improve the waveform fit compared to previous models. We find that data from the westernmost seismic stations used in this study require a shallower Moho depth (∼10 km) than data from stations in the eastern part of the archipelago (∼13–16 km). This apparent increase in the Moho depth with increasing distance from the mid-Atlantic ridge (MAR) is expected. However, the rate at which Moho deepens away from the MAR is greater than that predicted from a half-space cooling model, suggesting that local tectonic perturbations have modified crustal structure. The 1-D V_S models obtained beneath the westernmost seismic stations also show higher wave speeds than for the easternmost stations, which correlates well with the ages of the islands except Santa Maria Island. We interpret the relatively low V_S profile found beneath Santa Maria Island as resulting from underplating, which agrees with previous geological studies of the island. Compared to a recent receiver function study of the region, the shallow structure (top ∼2 km) in our models shows lower shear wave speed, which may have important implications for future hazard studies of the region. More generally, the new seismic crustal models we present in this study will be useful to better understand the tectonics, seismicity, moment tensors and strong ground motions in the region.

Key words: Surface waves and free oscillations; Crustal imaging; Atlantic Ocean; Composition and structure of the oceanic crust.

1 INTRODUCTION

The seismic structure of the crust beneath ocean island volcanoes gives key information about the mechanical and thermal properties of the oceanic lithosphere, the potential role of magmatic underplating and the controls of the crust on the formation of tectonic swells in marine settings (e.g. McKenzie *et al.* 2005; McNutt & Caress 2007). Moreover, a good knowledge of the shallow crustal structure of oceanic islands is crucial for reliable seismic hazard assessment, notably for accurate ground motion simulations (e.g. Olsen 2000), as well as for enhanced determinations of earthquake locations and focal mechanisms (e.g. Frietsch *et al.* 2018).

A wide range of active and passive seismic techniques can be used to map crustal structure. Popular methods include receiver

function analysis (e.g. Rondenay 2009), local earthquake tomography (e.g. Thurber 1993) and surface wave tomography methods using both earthquake and seismic ambient noise data (e.g. Shapiro *et al.* 2005). Early geophysical studies of the crustal structure of the Azores include active seismic studies (Hirn *et al.* 1980), which led to a 1-D seismic model of the region that is used in seismicity analysis by IPMA, the Portuguese seismic monitoring agency (e.g. IPMA 2016). Previous crustal thickness estimates beneath the archipelago are within the range ∼10–30 km (e.g. Detrick *et al.* 1995; Escartín *et al.* 2001), which is much thicker than typical oceanic crustal thickness (∼7 km; e.g. Mutter & Mutter 1993). Possible explanations for the observed thick crust include tectonic processes related to plate motions, the building of the Azores Plateau and the presence of a mantle plume, which may lead to magmatic intrusions or volcanic loading.

In the past two decades several temporary and permanent seismic stations have been deployed in the region, providing opportunities to study its seismic structure in detail. Silveira *et al.* (2010) computed receiver functions and estimated a Moho depth of 20–30 km in the region. However, this study mainly focused on mantle structure rather than on the region's fine crustal structure. Dias *et al.* (2007) conducted a local tomography study of the region near the Faial and Pico Islands, but their study region only represents a small portion of the archipelago. More recently, Spieker *et al.* (2018) investigated the crustal structure of the region using teleseismic *P*-wave receiver functions. They reported a Moho depth of ∼17 km throughout the archipelago and found evidence for possible magmatic underplating beneath the island of São Jorge, as well as some indications of underplating beneath São Miguel and possibly Santa Maria. However, the depth estimates obtained by Spieker *et al.* (2018) are potentially limited by multiples due to reverberations of converted phases reflected at the seafloor, as well as by limited backazimuthal coverage resulting from a relatively short recording period.

In this study, we invert teleseismic Rayleigh wave ellipticity measurements (the horizontal-to-vertical ratio of fundamental mode Rayleigh wave particle motion) for 1-D crustal shear wave velocity (V_S) profiles beneath five seismic stations in the Azores Archipelago. To the best of our knowledge, this is the first time that Rayleigh wave ellipticity data are used to determine the crustal structure of ocean island volcanoes. Prior to this study, the analysis of teleseismic Rayleigh wave ellipticity has been used to probe the crustal structure in continental regions (e.g. Lin *et al.* 2012; Berbellini *et al.* 2017; Attanayake *et al.* 2017). This was possible due to the strong sensitivity of Rayleigh wave ellipticity to the uppermost crustal V_S structure in the immediate vicinity of a seismic station (e.g. Tanimoto & Alvizuri 2006; Ferreira & Woodhouse 2007a, b; Tanimoto & Rivera 2008; Maupin 2017). Being a single-station measurement, Rayleigh wave ellipticity is particularly suited for illuminating crustal structure in regions with uneven seismic station coverage such as ocean islands, where application of seismic tomography is difficult. We test the reliability of our new V_S models by using them in moment tensor inversions of local seismic data from the 2013 April 30 M_w 5.9 earthquake in the Povoação basin near São Miguel Island. Moreover, we also perform such independent source inversion tests using other previous 1-D Earth models of the region. In the next section we provide a summary of the tectonic setting of the Azores, which is followed by our Rayleigh wave ellipticity analysis and validation against local earthquake data in Sections 3 and 4, respectively. Our results are then discussed in Section 5. Finally, we provide our conclusions in Section 6.

2 SEISMO-TECTONIC FEATURES OF THE AZORES ARCHIPELAGO

The Azores Archipelago is located near a triple junction where the Eurasian, North American and African (or Nubian) tectonic plates meet (Fig. 1). The eastern end of the North American plate is marked by the Mid-Atlantic ridge, while the boundary between the African and Eurasian plates is diffuse, including several faults and fracture zones (e.g. Miranda *et al.* 2014). The archipelago comprises nine islands sitting on the prominent Azores volcanic Plateau with its distinct triangular shape. Geographically, the islands are typically divided into: (i) the western group (Flores and Corvo); (ii) the Central Group (São Jorge, Faial, Pico, Graciosa and Terceira) and (iii) the eastern group (São Miguel and Santa Maria). The Azores Plateau has two different east and west sectors, whereby the larger eastern sector includes the Terceira ultra-slow spreading ridge, which includes Graciosa, Terceira and São Miguel Islands. To the east, the boundary between the Eurasian and African plates corresponds with the Gloria fault (Fig. 1).

A deep mantle plume has been proposed to contribute to the volcanism that led to formation of the Azores Islands (e.g. Schilling 1975; Silveira *et al.* 2006). It may have interacted with the mid-Atlantic ridge, leading to the high elevation of the Azores Plateau, which is roughly defined by a ∼2000 m isobath (e.g. Schilling 1975; Gente *et al.* 2003). Possible magmatic intrusions and underplating below the oceanic crust have been suggested to affect the eastern islands in the archipelago (e.g. Ramalho *et al.* 2017). Magmatic underplating results from large igneous intrusions at the bottom of the crust with seismic wave speeds that are higher than those typical of the lower crust, but lower than in the mantle (e.g. Caress *et al.* 1995). This has been observed in some volcanic ocean islands in the North Atlantic, such as the Cape Verdes and Canaries (e.g. Lodge & Helffrich 2006; Lodge *et al.* 2012). In the Azores, these geological processes have been proposed to cause the recent uplift of the easternmost island of the archipelago, Santa Maria (Fig. 1), which is also thought to be the oldest in the region (∼6 Ma; Sibrant *et al.* 2015; Ramalho *et al.* 2017). Recently, Spieker *et al.* (2018) used receiver functions to show that underplating occurs beneath São Jorge Island. They also found some indications that it may be present beneath São Miguel and Santa Maria, but additional data and analyses are needed to confirm these findings.

In the central and eastern groups of the archipelago, the youngest and most active islands are Pico, Faial, Terceira and São Miguel, whose age estimates range from 0.27 to 0.88 Ma (e.g. Chovelon 1982; Johnson *et al.* 1998; Calvert *et al.* 2006; Hildenbrand *et al.* 2012; Sibrant *et al.* 2015). On the other hand, São Jorge and Graciosa Islands, which are located to the west of these islands, are probably older, with age estimates in the range ∼1.05–1.85 Ma (e.g. Hildenbrand *et al.* 2008; Larrea *et al.* 2014; Marques *et al.* 2018). Finally, Flores and Corvo have been dated with ages ∼2.2 Ma (Azevedo & Portugal Ferreira 2006) and ∼1.5–1.0 (França *et al.* 2003), respectively. Hence, unlike other settings such as the Hawaiian-Emperor seamount chain, the Azores Archipelago does not exhibit a clear linear age trend. This highlights the complexity of the formation and evolution of the islands, which remain poorly understood.

The Azores Archipelago has significant seismicity; over 30 destructive earthquakes have occurred in the region since the 15th century (Gaspar *et al.* 2015). The most destructive historical earthquake in the Azores was the 1522 Vila Franca do Campo event in São Miguel Island (Gaspar *et al.* 2015), which had an intensity X (Silveira *et al.* 2003) and led to over 5000 casualties. More recent

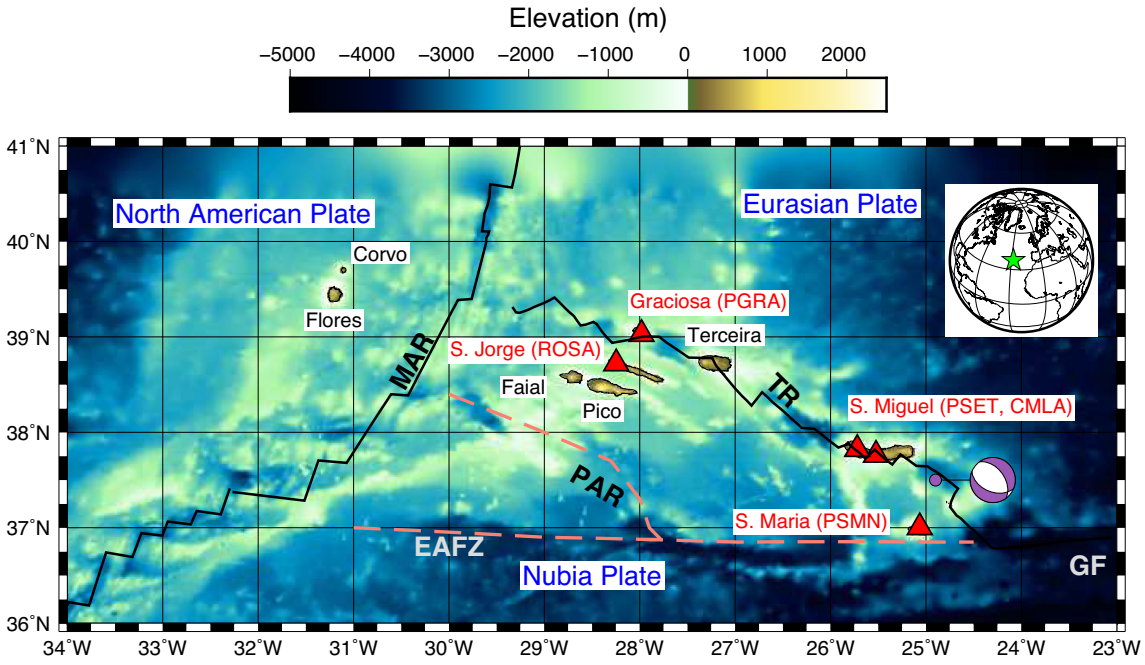

Figure 1. Tectonic setting and geographical location of the Azores Archipelago. The tectonic boundaries between the North American, Eurasian and Nubian plates are shown. Moreover, key tectonic features of the region are presented (e.g. Miranda *et al.* 2014): the Mid-Atlantic Ridge (MAR), the East Azores Fault Zone (EAFZ), the Princess Alice Rift (PAR), the Terceira Rift (TR) and the region of the Gloria fault (GF). The location and the focal mechanism of the 2013 April 30 M_w 5.9 Povoação basin earthquake is also shown (Frietsch *et al.* 2018) along with the seismic stations used in this study (red triangles; the corresponding island is also written in red, with the station name given in brackets). Topography and bathymetry are from SRTM30 PLUS (Becker *et al.* 2009).

significant earthquakes include the 1980 Mw 6.8 event west of Terceira Island, the 1997 M_w 5.9 earthquake SE of Terceira Island and the 1998 M_w 6.0 event in Faial (e.g. Borges *et al.* 2007). In the past decade, the largest magnitude event that occurred in the region was the 2013 April 30 M_w 5.9 earthquake with an epicentre in the Povoação basin, near São Miguel Island (Fig. 1). While this event did not produce substantial damage (USGS 2017), it was recorded by a number of seismic stations in the region, bringing useful information about the tectonics of the archipelago. In particular, this earthquake exhibited a substantial non-double couple component, which is possibly due to a curved fault in the complex active fault system of the Povoação basin (Weiß *et al.* 2015; Frietsch *et al.* 2018).

3 TELESEISMIC RAYLEIGH WAVE ELLIPTICITY ANALYSIS

3.1 Data

We use seismic waveforms from five permanent broadband seismic stations in the Azores: ROSA, PGRA, PSET, CMLA and PSMN (Fig. 1) recorded in the period between January 2009 and February 2015. Station CMLA in São Miguel Island is part of the Global Seismographic Network (GSN), while the other stations are all run and maintained by IPMA. We use recordings of 414 earthquakes with M_w 6.0–7.8 and with good azimuthal distribution (Fig. 2). Epicentral distances between 50° and 120° are considered to avoid the interference of multiple orbit waves and to reduce near-source effects. A list of these earthquakes is given in Table S1 in the Supporting Information. We use the fully automated, time-domain measurement scheme of Attanayake *et al.* (2017) to measure Rayleigh wave ellipticity (RWE) with central wave periods ranging from 15 to 60 s with an interval of 5 s. With this procedure we obtain between 34 and 329 measurements per period, per station. The maximum wave period used in this study ($T \sim 60$ s) is determined by the response spectra of the seismometers used in this study. Other seismic stations in the region had fewer measurements (less than 30 measurements) due to short recording period or noisy recordings; hence, they were considered unreliable and were discarded. As explained in detail in Attanayake *et al.* (2017), a number of quality control measures are applied to ensure that fundamental mode Rayleigh wave ellipticity measurements are properly isolated. These include: (i) the phase shift between the vertical component and the Hilbert-transformed radial component waveforms must be in the range between 70° and 90° (phase shifts greater than 90° are folded back into the 0°–90° range); (ii) the cross-correlation coefficient between the two waveform components must exceed 0.8 and (iii) RWE measurements outside the 0.2–2 range are cut-off to avoid unrealistically anomalous subsurface velocity values. These three quality control criteria ensure that only seismograms with highest signal-to-noise ratio (SNR) are retained and we did not observe systematic variations of SNR with backazimuth or distance. Fig. 3 shows the distribution of the logarithm of the measurements for the five seismic stations considered in this study. These are smooth and show near-Gaussian behaviour. Fig. 4 shows the geographical distribution of the median of the measurements as a function of wave period. RWE decreases with increasing wave period and we observe that there is a tendency for slightly larger RWE measurements in the eastern islands (PSET, CMLA and PSMN) than in the western islands (ROSA and PGRA).

3.2 Inverting for 1-D shear-velocity structure

We use the inversion scheme of Berbellini *et al.* (2017) and Attanayake *et al.* (2017) to invert the RWE measurements for 1-D V_S

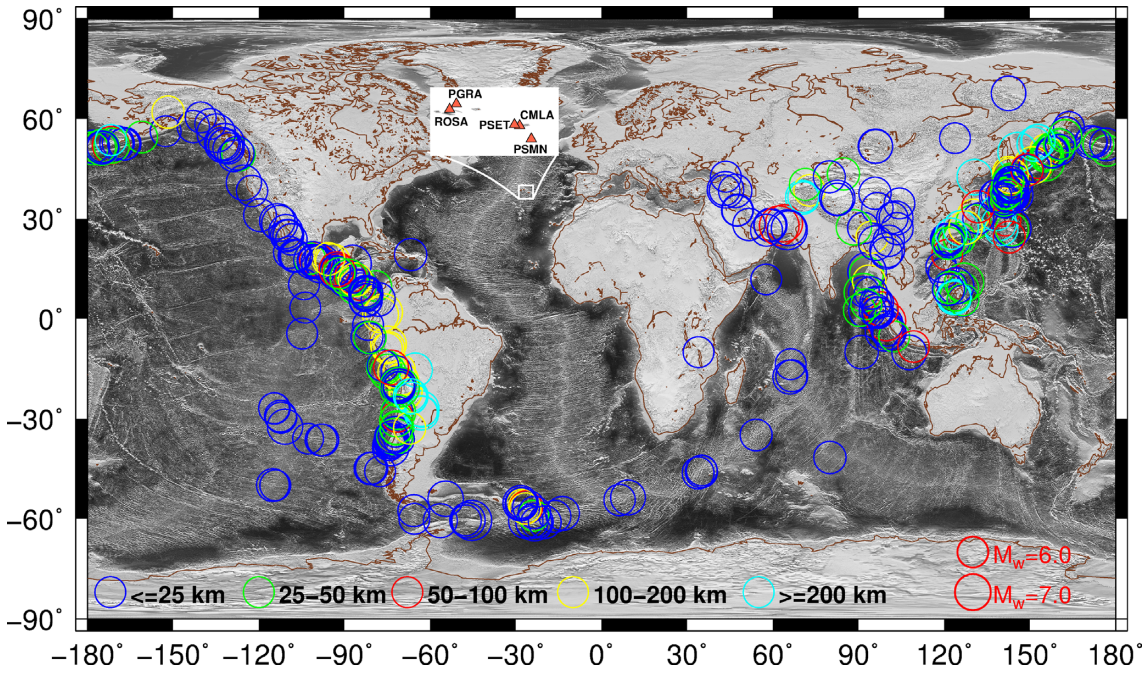

Figure 2. Distribution of 414 earthquakes (circles) used in this study. The size of the circles depends on the magnitude of the events (M_w 6.0–7.8) and they are colour-coded by depth. The white box shows the study region, including the five stations used in this study.

structure beneath the five seismic stations in the Azores used in this study. The inversion uses the neighbourhood algorithm (NA; Sambridge 1999), which is based on a fully non-linear, self-adaptive Monte Carlo approach. The NA samples the model space efficiently, leading to an ensemble of Earth models that are classified according to their associated cost function value. In addition to examining the formally best-fitting model obtained from the inversion, we also plot all the models with data misfit values within 20 per cent of the minimum misfit value obtained from the inversions. This enables us to empirically assess model uncertainties (Berbellini *et al.* 2017; Attanayake *et al.* 2017). The 20 per cent threshold is chosen such that it includes models that fit the RWE measurements reasonably well. While a stricter threshold leads to a limited number of models which are not necessarily representative, a looser threshold includes models with poor data fits.

Our inversion scheme minimizes the cost function:

$$c = \sum_{i=1}^{N_m} \frac{(d^i_{obs} - g^i(\mathbf{m}))^2}{(\sigma^i_D)^2} + AN_m \sum_{j=1}^{N_l} (V_S^{j-1} - 2V_S^j + V_S^{j+1}), \quad (1)$$

where d_{obs} is the observed RWE measurement, $g(\mathbf{m})$ is the predicted RWE value for the sampled model $\mathbf{m}$, σ_D is the variance of the measurement, N_m is the number of measurements, N_l is the number of layers in the model parametrization, A is a scaling factor, and V_S^j is the shear wave velocity at layer j. The first term in eq. (1) represents the misfit between the RWE observations and the theoretical predictions for the specific candidate model m. We follow the usual assumption that the measurements have uncorrelated Gaussian variance σ_D^2. The second term in eq. (1) defines the second derivative of the candidate V_S model. The inversion procedure samples the model space with the aim of minimizing the misfit to the observed data while favouring smooth models. This is important to avoid unrealistic complex models that may fit the data well. Indeed, we performed inversions with and without this second regularization term and found that it is key to stabilize the inversions, otherwise we could obtain oscillatory, unphysical models. While by using regularization we are potentially discarding complex models, it is likely that the data used cannot constrain very complex models alone. The A factor is chosen by trial and error; the larger the A factor the larger the penalty given to rough models. Having tested a large number of A factors, we found that using $A = 10^{-4}$ km^{-1} led to relatively smooth models that fit the data well. This amount of regularization is relatively modest and hence we are not imposing too strong constraints on the models.

Theoretical RWE values $g(\mathbf{m})$ are computed using a normal mode formalism (Gilbert 1971) by using the software package of Herrmann (2013), which enables the fast and efficient calculation of normal mode eigenfunctions and eigenvalues numerically in 1-D layered media.

The inversion algorithm uses two tuning parameters: (i) the number of models created in each iteration, n_s and (ii) the number of best models, n_r, around which the algorithm will continue to search. After trying several values for n_s and n_r, we found that convergence was achieved after trying 1500 models when using $n_s = 20$ and $n_r = 5$.

Given our lack of knowledge of the detailed layered crustal structure of the Azores, we started by using the four-layer parametrization of Lin *et al.* (2012) with some modifications, which was also successfully used by Attanayake *et al.* (2017). Specifically, the uppermost layer of the crust has a fixed thickness of 1.5 km and the thickness of the second layer is fixed to 4 km. The thickness of the two bottom layers is then given by half the difference between the Moho depth and 5.5 km. We explored the sensitivity of the inversions to Moho depth by performing several inversions whereby the Moho depth was successively fixed to different values in the range 5.5–30 km, with steps of 5 km and then finer steps were considered around the best-fitting models. For each station we chose the model with the lowest cost function obtained from a stable inversion as our favourite model. We found that the inversions for stations ROSA

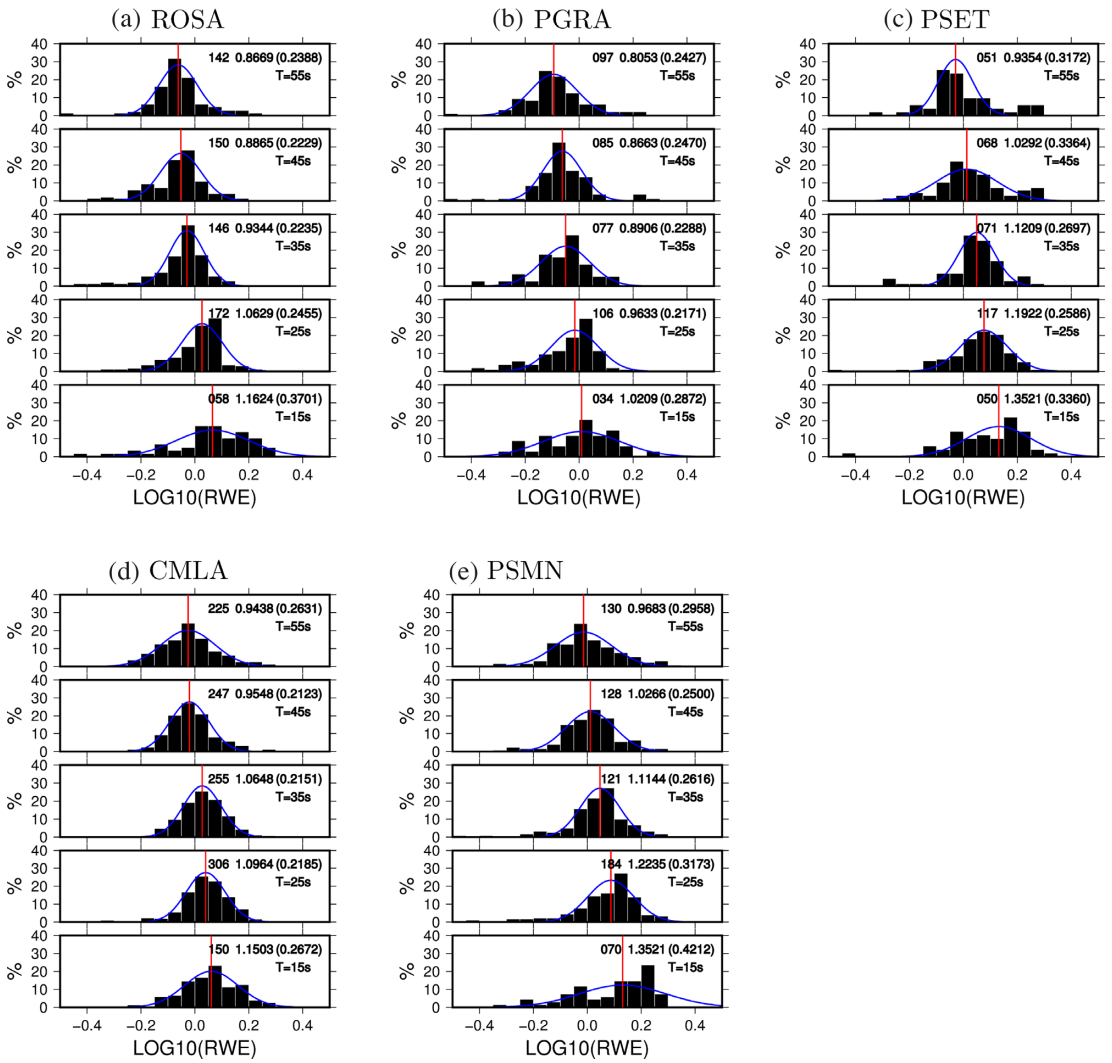

Figure 3. Distribution of the Rayleigh wave ellipticity (RWE) values measured in this study for the five seismic stations considered. Near-Gaussian distributions of RWE are observed for all wave periods. Each diagram also shows the number of observations, the median and the uncertainty, respectively, along with the corresponding wave period. The red vertical line indicates the median value and the blue curve shows the equivalent Gaussian distribution.

and PGRA required shallower Moho depths (∼10 km) than for the other stations. When using Moho depths larger than ∼10 km, the data fits for stations ROSA and PGRA were not only poor, but also the inversions were unstable. Thus, for stations ROSA and PGRA we use a three-layer parametrization with layer thicknesses of 2 km (top layer), 3 km (middle layer) and 5 km (bottom layer). These layer thicknesses were chosen by trial and error to stabilize the inversions. Table S2 in the Supporting Information summarizes the parametrization used for each station and the range of V_S values searched within each crustal layer for each station. For completeness, we also carried out exploratory joint inversions for Moho depth and for V_S in each layer. We found that while the results from the joint inversions for Moho depth and V_S were very similar to those obtained successively fixing the Moho depth at different values, the former inversions were more unstable than when inverting only for V_S. Future work combining Rayleigh wave ellipticity with, for example receiver function data may help improve joint inversions for Moho depth and V_S. Below the Moho, we fixed the structure to that of LITHO1.0 (Pasyanos *et al.* 2014). We also performed inversion experiments including an upper mantle layer, but we found that in general it led to unstable results. Hence, despite the theoretical broad sensitivity of RWE data to both crustal and upper mantle structure (e.g. Lin *et al.* 2012; Shen & Ritzwoller 2016), we found that our data set cannot constrain the latter.

We only invert for V_S, which is used to calculate the compressional wave velocity (V_P) and density (ρ) applying the empirical scaling relations of Brocher (2005) for the crust.

3.3 Results

3.3.1 Shear wave velocity models

Fig. 5 shows the results from the inversions of the Rayleigh wave ellipticity (RWE) data for the five stations in the Azores considered in this study, where the best-fitting model is shown in green and the models with misfit values within 20 per cent of the minimum misfit are shown in black (Table S3 in the Supporting Information also presents the corresponding model values). For completeness we also present the minimum and maximum values of the cost functions of the models shown in black and we also present the

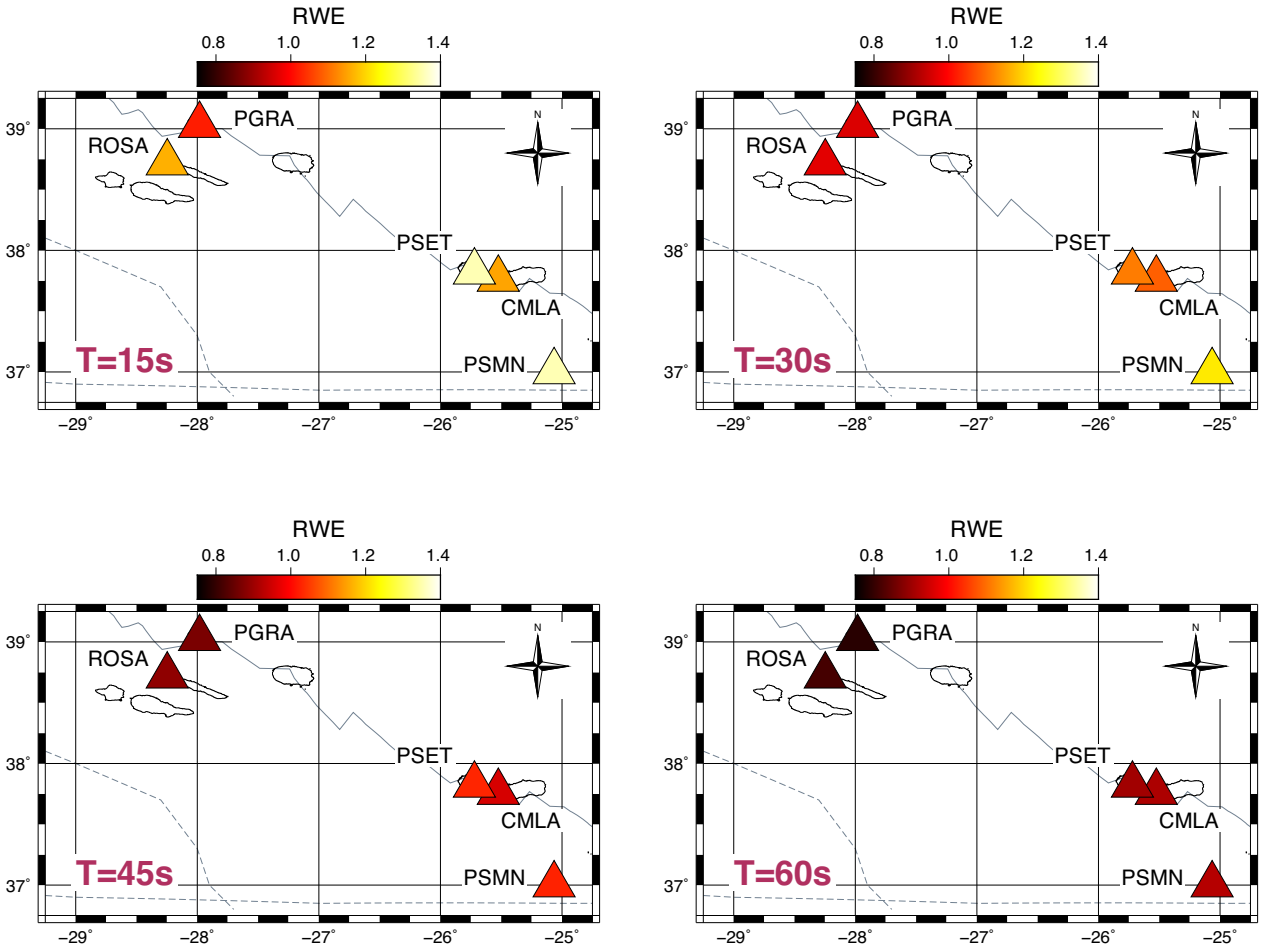

Figure 4. Geographical distribution of the Rayleigh wave ellipticity (RWE) measurements obtained for the five stations considered for four illustrative wave periods. There is a tendency of lower RWE values for the two westernmost stations (ROSA and PGRA) than for the other stations.

number of posterior models. As explained above, the range of V_S values shown in black gives an empirical estimate of the model uncertainties. While the errors for stations PSET, CMLA and PSMN are generally small (∼0.24–0.49 km s^{-1}), they are larger for stations ROSA and PGRA (∼0.53–1.48 km s^{-1}). Fig. 6 illustrates the comparison between the measured RWE curves and the predictions from the best-fitting models shown in Fig. 5, showing excellent fit to the data. As explained in the previous section, we found that the RWE data inversions required shallower Moho depths for stations ROSA and PGRA (Moho depth ∼10 km) than for stations PSET, CMLA and PSMN, for which we obtained best-fitting Moho depths between ∼13 km and ∼17 km (Fig. 5). These latter stations also show the lowest shear wave velocity values in the top layer (∼1.4–1.7 km s^{-1} compared to ∼1.7 and 2.6 km s^{-1} for stations ROSA and PGRA, respectively). Fig. 5 shows that at ∼3 km depth, the shear wave velocity varies in the range ∼2.4–3.3 km s^{-1}, which then increases to ∼3.1–3.9 km s^{-1} at 8 km depth. At this depth, the westernmost stations (PGRA and ROSA) show the highest shear-wave speeds. Finally, at 12 km depth, the stations PSET, CMLA and PSMN show V_S values in the range ∼3.6–4.0 km s^{-1}. The maps in Fig. 7 also show clearly that overall there is a tendency for faster shear wave speed beneath the westernmost stations ROSA and PGRA than for the other stations. For completeness, Fig. S1 shows the geographical distribution of the best-fitting Moho depths found in this study.

In order to investigate potential trade-offs between V_S in the various layers, we plot the ensemble of model parameters sampled against each other in Fig. 8 for station CMLA (the corresponding plots for all the other stations are shown in Figs S2–S5 in the Supporting Information). The best-fitting model is marked by a green cross, models with misfit values within 20 per cent of the best-fitting model are plotted as black dots and the dots in grey correspond to all the models sampled. If there is a trade-off between V_S in any pair of layers, the cloud of black points should show a diagonal distribution. This is not observed for station CMLA; the models in black are located mostly in tight clusters around the best-fitting solution. The same applies to the other stations, apart for stations PGRA (Fig. S2) and ROSA (Fig. S3), which show some trade-offs between V_S in adjacent layers.

As explained in Section 3.2, we also performed exploratory inversions jointly inverting for V_S and for Moho depth. Fig. S6 shows the evolution of the cost function as a function of the number of models sampled for station CMLA when inverting solely for V_S (left-hand panel) and when inverting jointly for V_S and for Moho depth (right-hand panel), which highlights that the latter inversions were more unstable, with more high misfit mod-

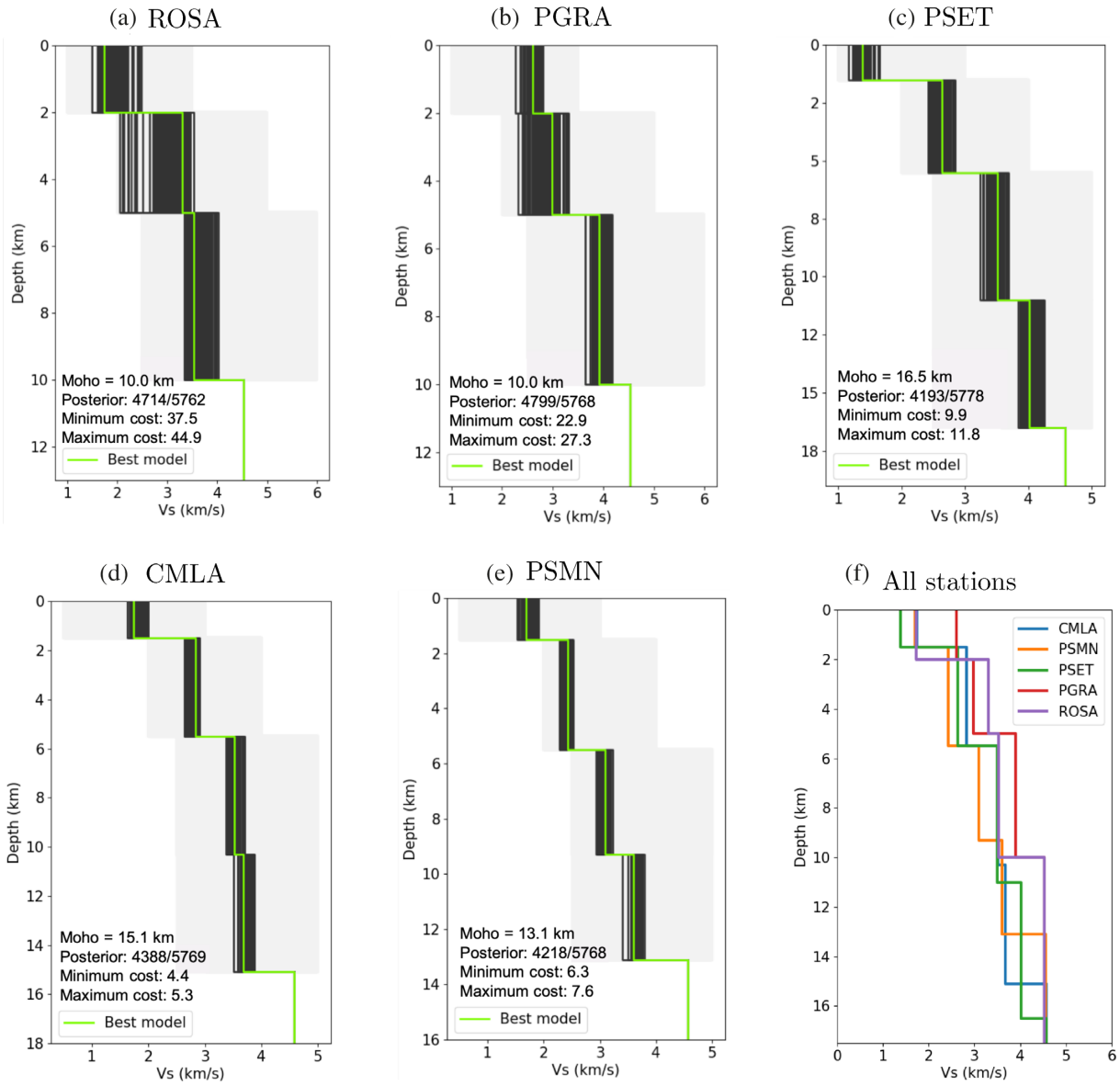

Figure 5. V_S profiles obtained from the inversion of our RWE measurements for the five seismic stations used in this study. The profile in green corresponds to the formally best-fitting model. The models in black lead to data misfit values within 20 per cent of the best-fitting model. The models in grey are all the models sampled in the inversion process. The preferred Moho depths found for each station are annotated in each subplot as well as the minimum and maximum values of the cost functions of the models shown in black and the number of posterior models compared to the total number of models sampled (see main text for details). All the best-fitting models are compared in (f).

els occurring during the inversion process. Fig. S7 shows the corresponding models obtained from the joint inversion for V_S and for Moho depth, which are similar to those presented in Fig. 5(d).

3.3.2 Comparison with Rayleigh wave ellipticity predictions from receiver function models

In order to further compare our new 1-D V_S models quantitatively with existing 1-D models of the Azores Archipelago, we compute the predicted RWE using the receiver function 1-D crustal models of Silveira *et al.* (2010) and of Spieker *et al.* (2018). Fig. 9 compares these RWE predictions with observations, as well as with the predicted RWE curve for our best-fitting model for CMLA station (see Fig. 5). While all the models fit the long-period data ($T \geq 45$ s) within the data uncertainty range, none of the receiver function models fit the observed short-period RWE data ($T \leq 30$ s) well. Amongst the various receiver function models considered, the model Spieker-M7c leads to the predictions that are closest to the RWE observations.

4 VALIDATION AGAINST INDEPENDENT LOCAL EARTHQUAKE DATA

4.1 Local earthquake data

In order to independently test the reliability of the crustal models obtained in this study from teleseismic RWE data, we examine how

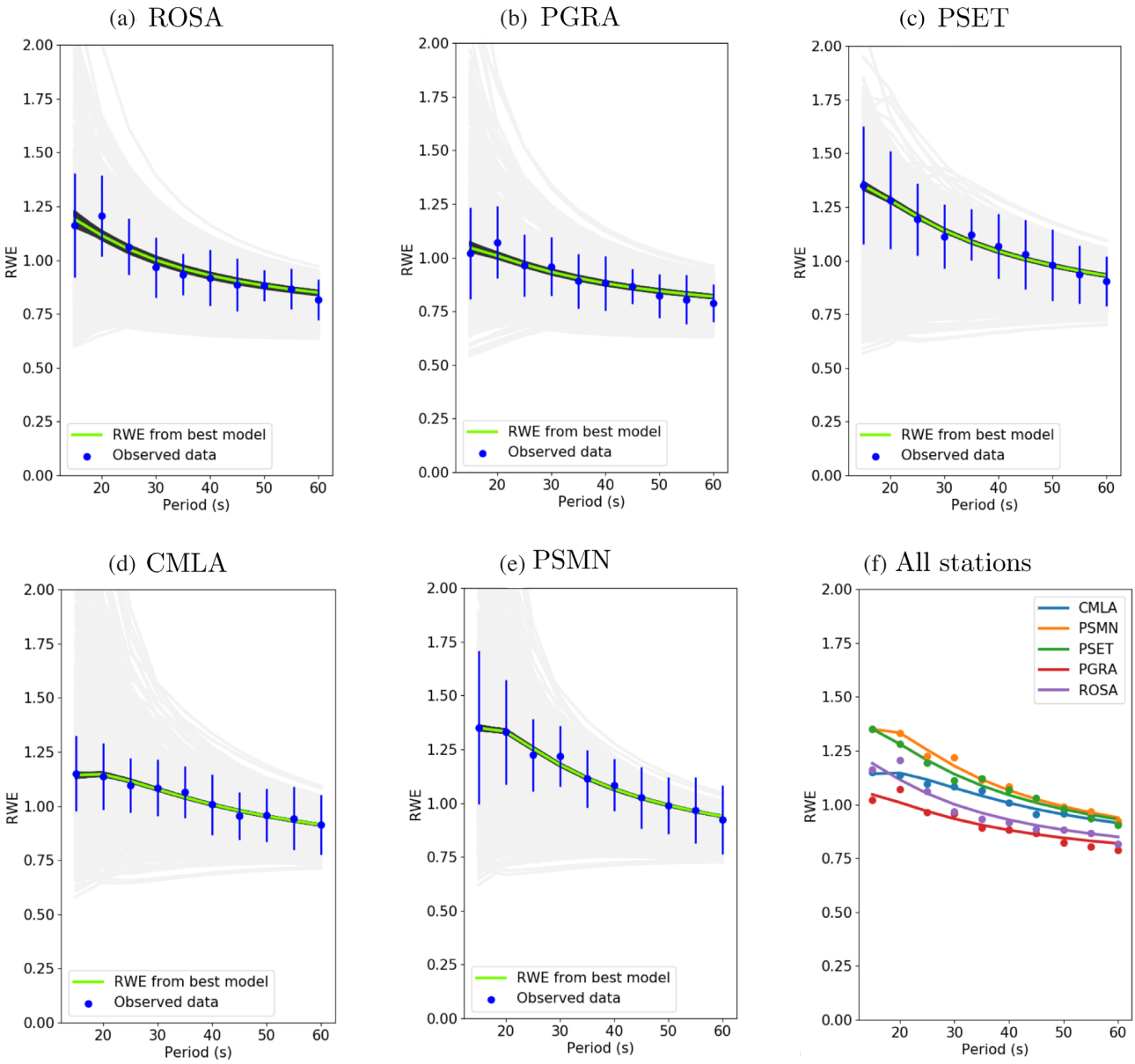

Figure 6. Comparison between our RWE observations (blue dots with error bars) and predictions for the best-fitting models shown in Fig. 5 (green). The predicted RWE curves for the models within 20 per cent of the best-fitting models are also shown (black curves) as well as for all the models sampled in the inversion process (grey lines). The RWE measurements (dots) and predictions for the best-fitting models (solid lines) for all five stations are compared in (f).

well they explain independent seismic data that were not used to obtain the RWE measurements. Specifically, we use our new 1-D crustal models in moment tensor inversions of local seismic waveforms recorded in the Azores Archipelago following the 2013 April 30 M_w 5.9 earthquake in the Povoação basin (Fig. 1). As mentioned previously, this event is the largest magnitude earthquake that occurred in the Azores Archipelago in the past decade and it produced high-quality waveforms (Frietsch *et al.* 2018). Having evaluated the signal-to-noise ratio across a range of frequency bands, the local seismic waveforms are bandpass filtered in the period range 17–33 s to ensure good quality signals compatible with our modelling. In order to clearly isolate the main arrivals, we cut the seismic waveforms with a window length of 256 s. The traces in black in Fig. 10 show the observed seismic waveforms, which are compared with theoretical seismograms in red; the comparisons between observed and theoretical seismograms will be discussed in Section 4.4.

4.2 Earth models

We test the five new 1-D crustal models obtained in this study by verifying how well they explain local earthquake waveforms recorded in the Azores compared to other existing models of the region. In addition to the new 1-D crustal models obtained in this study, we also use the following existing models of the region in our modelling: (i) CRUST2.0 (Bassin *et al.* 2000); (ii) IPMA, which is used by IPMA in their routine seismicity and moment tensor inversions (adapted from Hirn *et al.* 1980); (iii) PREM (Dziewoński & Anderson 1981); (iv) *P*–*S* CMLA and *P*–*S* CMLAc (Silveira *et al.* 2010), which are based on *P* and *S* receiver functions computed for station CMLA, where the 'c' in the model name means that the receiver function inversion included traveltime corrections; (v) *P*–*S* COSEAa and *P*–*S* COSEAc, which were obtained from *P* and *S* receiver functions from stations from the temporary seismic

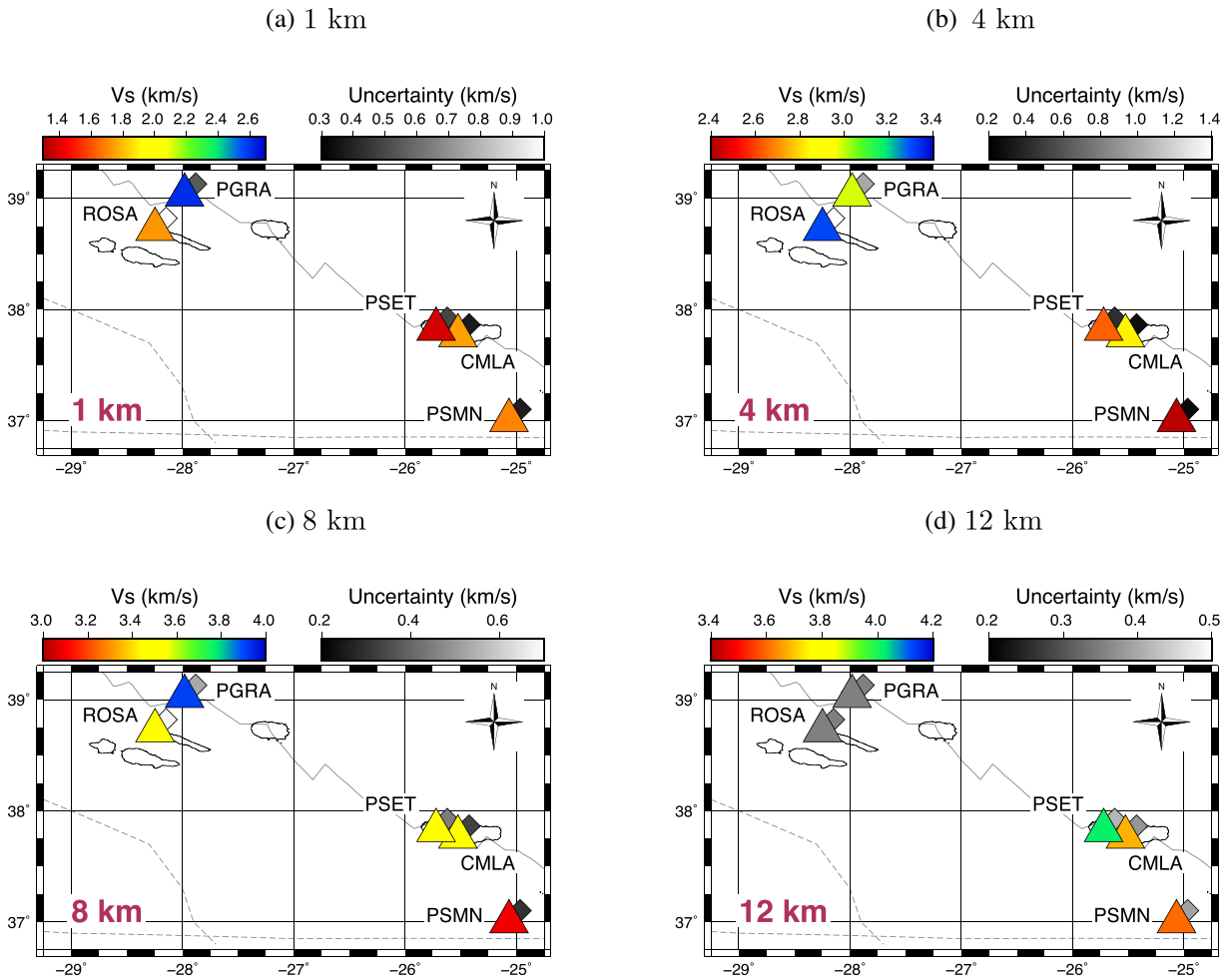

Figure 7. Geographical distribution of the V_S values obtained in this study (triangles) as well as their uncertainties (diamonds) for depths of 1, 4, 8 and 12 km. There is a tendency for slightly larger V_S values for the westernmost stations, notably for station PGRA. Note that the best-fitting Moho depth for stations ROSA and PGRA is ∼10 km; hence, there is no crustal V_S value for these two stations at 12 km depth.

network COSEA that included five stations in Santa Maria, Graciosa, Terceira, Pico and Corvo Islands (Silveira *et al.* 2010); (vi) P-SKS CMLAa and P-SKS CMLAc based on *P* and SKS receiver function inversion (Silveira *et al.* 2010) and (vii) Spieker-M7a and Spieker-M7c obtained by Spieker *et al.* (2018) from the analysis of teleseismic *P*-wave receiver functions for stations CMLA and ROSA using more and higher frequency data than Silveira *et al.* (2010). Thus, in total, we perform seismic moment tensor inversions using sixteen different 1-D earth models of the Azores region. Fig. 9 (left-hand panel) compares these various 1-D V_S models.

4.3 Moment tensor inversions

We use the software package ISOLA (Sokos & Zahradník 2008, 2013) to carry out moment tensor inversions of the 30 April 2013 M_w 5.9 Povoação earthquake using the earth models described in the previous section.

The ISOLA package is an efficient and user-friendly code that simulates full body and surface waveforms using Green's functions computed for a 1-D layered medium based on the discrete wavenumber method of Bouchon (1981). Least-squares inversions are performed in the time domain, which minimize the L_2-norm misfit difference (m_f) between the observed (**d**) and synthetic (**s**) waveforms:

$$m_f^2 = \frac{(\mathbf{s}-\mathbf{d})^T(\mathbf{s}-\mathbf{d})}{\mathbf{d}^T\mathbf{d}} \,. \quad (2)$$

The inversions are carried out for multiple realizations of the space–time centroid location (including the source depth) using a grid-search scheme. In this study we compute seismic waveforms with a maximum frequency of 0.1 Hz for the M_w 5.9 Povoação earthquake recorded in the seismic stations in the Azores, which are located at epicentral distances between 61 km (CMLA station) and 322 km (ROSA station). The synthetic seismograms are filtered exactly in the same way as the real data (see Section 4.1).

4.4 Results

Fig. 11 shows the focal mechanisms and the associated variance reductions ($V_r = 1 - m_f$, where m_f is the L_2-norm misfit in eq. (2)) obtained from the moment tensor inversions of the M_w 5.9 Povoação earthquake for the majority of 1-D earth models considered (see Table S4 in the Supporting Information for a list of the source parameters and variance reductions obtained for all 16 models). All the inversions lead to normal faulting focal mechanisms consistent with the solutions obtained by Frietsch *et al.* (2018). Fig. 11 shows that while all the 1-D earth models show relatively high variance

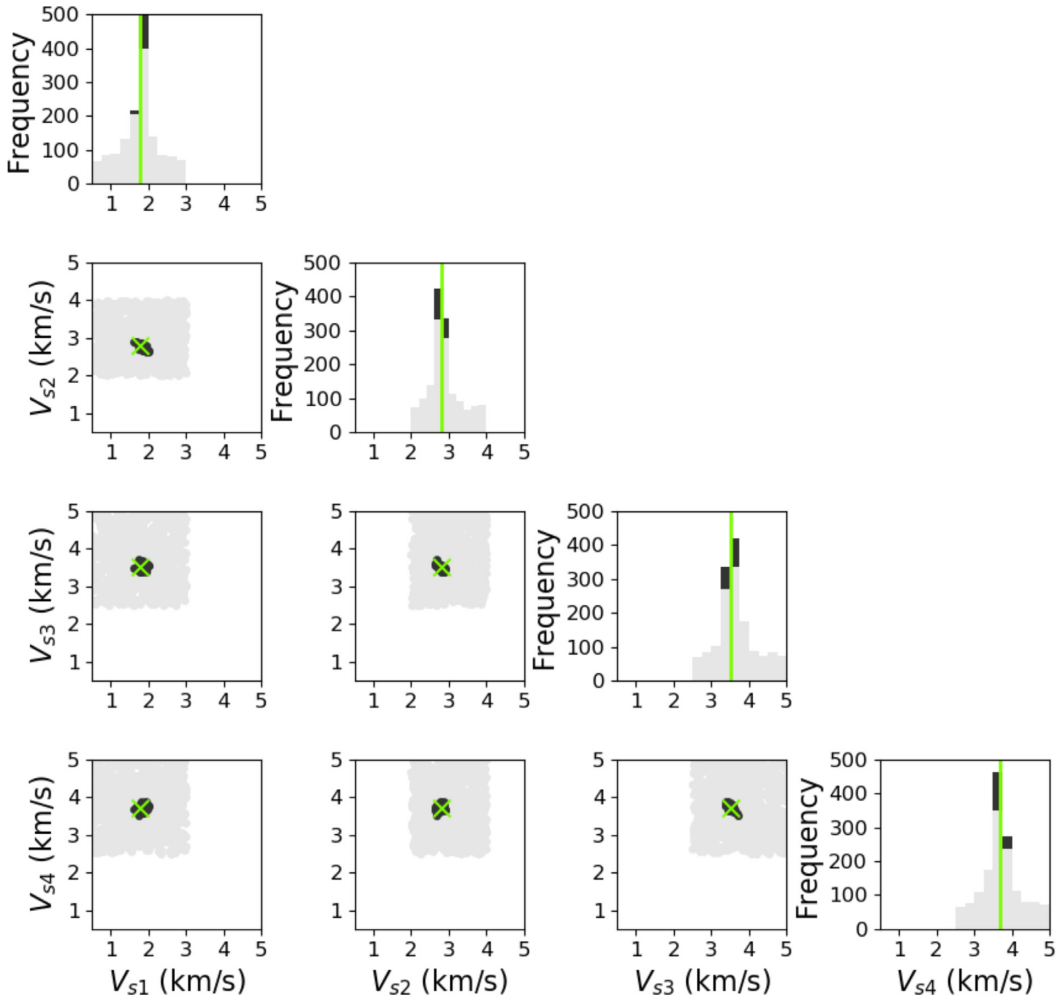

Figure 8. Scatter plots and distributions of all the V_S parameters in the four layers used in the RWE inversions for station CMLA. The best-fitting solution is marked by green crosses and vertical green lines. The parameters that correspond to solutions within 20 per cent of the best-fitting model are shown in black; all the other model parameters shown are in grey. Trade-offs between parameters would appear as diagonal features in the scatter plots.

reductions (larger than 78 per cent in all cases), the models *P–S* CMLAc and CRUST2.0 (VR = 78–80 per cent) produce the poorest data fits. On the other hand, the 1-D crustal V_S models CMLA_ell, PSET_ell and PSMN_ell that were obtained in this study perform best (VR = 85–87 per cent). Fig. 10 shows an illustrative example of waveform comparisons between the observations and the theoretical waveforms computed for the best-fitting source model obtained using our new 1-D V_S profile for station CMLA (CMLA_ell), which highlights the excellent data fit achieved. Thus, these tests show that our new 1-D crustal models of the Azores are reliable and useful for investigating the region's seismicity (e.g. hypocentral locations, moment tensors, etc.). Given that all the retrieved source models are very similar, the improved data fit obtained for our new 1-D models is likely due to the resulting enhanced Green's functions. Table S4 in the Supporting Information shows that the fault geometry parameters retrieved from the various inversions have a variability in fault strike of ∼34°, ∼8° in fault dip angle, ∼47° in rake, 10 km in depth, 1.4 s in centroid time and ∼26 per cent in double-couple component. This is similar to the variability in source parameters in the region reported by Frietsch *et al.* (2018) and is also compatible with the typical uncertainties in moment tensor solutions in seismic catalogues (e.g. Weston *et al.* 2011, 2012).

5 DISCUSSION

5.1 Crustal V_S structure

We found that the stations located in the westernmost islands considered in this study (station PGRA in Graciosa Island and station ROSA in São Jorge Island, which are ∼41 km apart) in the Azores Archipelago show the fastest 1-D V_S profiles (e.g. Fig. 7). As it was mentioned previously, Graciosa and São Jorge Islands are the oldest islands in the archipelago considered in this study after Santa Maria and, thus, in principle have been cooling for longer than other islands. On the other hand, stations CMLA and PSET (located in São Miguel Island) and PSMN (located in Santa Maria) show slower V_S profiles than PGRA and ROSA, with Santa Maria Island showing the lowest V_S values in the uppermost 12 km of the crust. While this may seem at odds with the estimated older age of Santa Maria than other islands, it is consistent with recent suggestions of substantial magmatic intrusions driving island uplift (Ramalho *et al.* 2017). Alternatively, geomechanical processes such as porosity development and thermal stressing can reduce the strength of volcanic rocks and thus V_S (Loaiza *et al.* 2012; Kendrick *et al.* 2013). As expected, the 1-D V_S profiles for stations CMLA and PSET are quite similar, notably in the top ∼10 km, since they

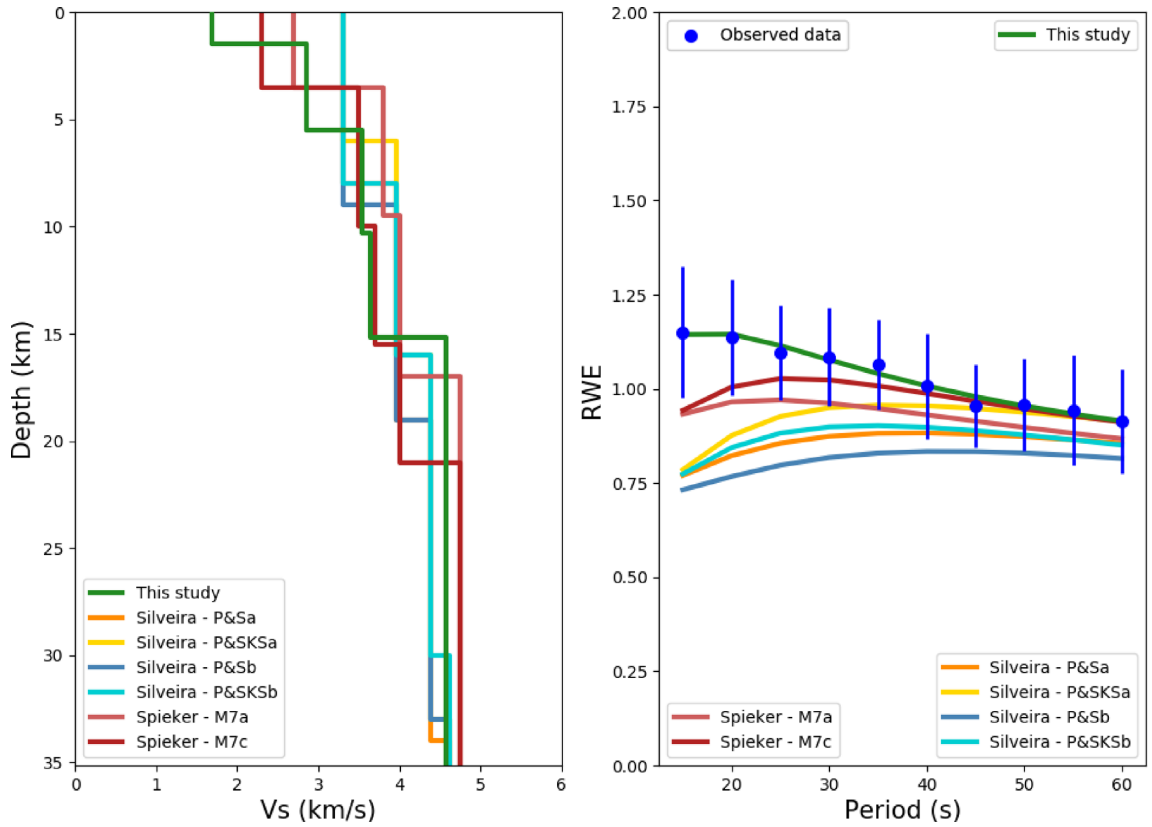

Figure 9. Left-hand panel: comparison between the various 1-D earth models used in our source inversions. 'This study' refers to the CMLA_ell model obtained in this study; the various models starting with 'Silveira' are from Silveira *et al.* (2010) and the two models starting with 'Spieker' are from Spieker *et al.* (2018). Right-hand panel: comparison between our RWE observations for station CMLA (blue dots with error bars) and the predicted RWE curves for the 1-D models shown on the left.

are located in the same island (São Miguel) being ∼18.5 km apart. Stations PGRA and ROSA show the largest uncertainties in V_S and parameter trade-offs. Since the RWE data uncertainties for PGRA and ROSA are among the lowest along with CMLA and we have processed the data using a uniform and consistent workflow, this suggests that the true V_S profiles below PGRA and ROSA are more complex than can be captured by our simple four-layer parametrization of the crust. This should not be a surprise given that Azores is undergoing constant modification through magma injection as explained previously. Further investigation is required to resolve this issue in the future considering models of complex crustal structure resulting from magma injections and using complementary imaging methods.

Comparing our new 1-D V_S models with the two preferred 1-D crustal models obtained from receiver function data by Spieker *et al.* (2018) (model Spieker-M7c for station ROSA and Spieker-M7a for station CMLA), we find that the top layer in our 1-D profiles tends to be slower than in Spieker et al.'s models (Fig. 9, left-hand panel). This shallow lower V_S layer, where RWE sensitivity is optimum, is a robust feature required to fit the short-period RWE data (Fig. 9, right-hand panel). This discrepancy may be at least partly due to limitations in constructing receiver functions to probe the crust beneath ocean islands. For example, the signals can be contaminated by shallow reverberations of converted phases beneath the island that can be reflected at the seafloor surrounding the island, leading to multiples. Future work using RWE measurements from seismic ambient noise data going down to shorter wave periods should enable us to obtain further detailed models of the shallow crust in the region (e.g. Hobiger *et al.* 2013; Berbellini *et al.* 2019), which are important to improve seismic hazard assessments.

The RWE predictions from models Spieker-M7c and Spieker-M7a fit the observations from station CMLA at $T \geq 45$ s well. These long-period RWE measurements are sensitive to deeper crustal structure (e.g. Berbellini *et al.* 2019) and, thus, the good agreement of RWE predictions based on different types of models gives confidence on the robustness of the deeper crustal structure obtained from our RWE inversions. The model Spieker-M7c fits the CMLA data slightly better than Spieker-M7a, which is somewhat surprising, given that it was built using data from station ROSA in São Jorge Island rather than from CMLA in São Miguel. This may be due to the fact that *P*-wave receiver functions typically constrain V_P better than V_S, whereas RWE has strong sensitivity to V_S. On the other hand, in the top 15 km, the models of Silveira *et al.* (2010) show substantial discrepancies to our models as well as to those of Spieker *et al.* (2018), displaying larger V_S values (Fig. 9). These discrepancies are not very surprising given that Silveira et al's models were built primarily to constrain mantle structure rather than crustal structure.

5.2 Moho depth

Our results show that the Moho depths beneath the two westernmost stations used in this study (ROSA and PGRA) are shallower than for the other stations (∼10 km compared to ∼13-17 km for the stations further east). Note that the five stations we use here are located

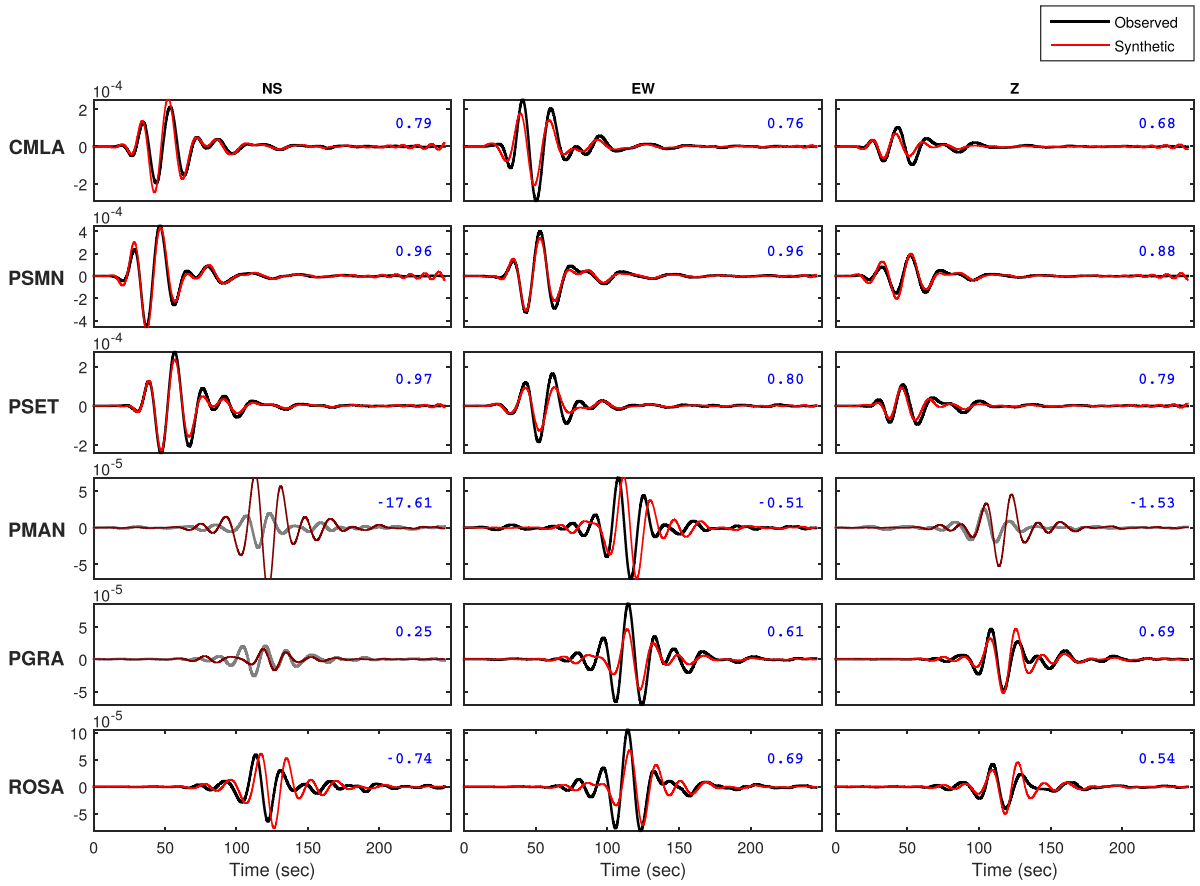

Figure 10. Local three-component waveform examples for the 30 April 2013 M_w 5.9 Povoação basin earthquake. Comparison of theoretical seismograms (red) with observed waveforms (black) for six three-component stations in the Azores. The synthetic seismograms are computed for source parameters obtained in this study using our best-fitting 1-D V_S model beneath station CMLA. The blue numbers correspond to the variance reduction V_r ($V_r = 1 - m_f$, where m_f is the L_2-norm misfit in eq. (2); see the main text). Traces in grey are not used in the source inversions due to their negative or low variance reduction. We note that station PMAN, which is located in São Jorge Island, was not used in the Rayleigh wave ellipticity analysis because it did not provide long enough recordings for the analysis.

between ∼150 km (ROSA) and ∼490 km (PSMN) from the Mid-Atlantic ridge, with the stations closest to the plate boundary having shallower Moho depths. Thus, the deepening trend of the Moho away from the plate boundary appears to be consistent with expectations from plate cooling models (e.g. Parsons & Sclater 1977; Stein & Stein 1992). Combining Stein & Stein (1992)'s GDH1 half-space equivalent plate model and Müller *et al.* (2008) seafloor ages, we estimate that the seafloor depth should increase by about 1 km from ROSA (west-end) to PSMN (east-end, see Supporting Information). If the seafloor depth varies linearly with Moho depth, this suggests that our models overestimate Moho depth variation away from the plate boundary. Such differences between theoretical predictions and empirical estimates are not surprising and can partly be attributed to local perturbations to the ambient thermal structure of the plate (e.g. Rychert & Harmon 2018). Our results suggest that perturbations to crustal thickness are accentuated near ocean islands, where significant magmatic activity takes place (e.g. Métrich *et al.* 2014; Zanon 2015; Ramalho *et al.* 2017). This has been suggested also for the Cape Verde archipelago in the Atlantic (see Ramalho *et al.* 2010a, b).

The best-fitting Moho depths found in this study broadly agree with estimates of 8–12 km from active seismic surveys, gravity and local earthquake tomography (e.g. Searle 1976; Escartín *et al.* 2001; Luis & Neves 2006; Dias *et al.* 2007) as well as with the more recent estimates of ∼15–17 km by Spieker *et al.* (2018). On the other hand, as pointed out by Spieker *et al.* (2018), Silveira *et al.* (2010) estimated larger Moho depths of ∼20–30 km for the region, which are not compatible with the Rayleigh wave ellipticity data obtained in this study. The deeper Moho depths obtained by Silveira *et al.* (2010) are probably due to the dominant lower frequency content of their data compared with Spieker *et al.* (2018).

5.3 Underplating

As explained in the introduction, crustal underplating has been suggested to explain the significant recent uplift of Santa Maria Island (Ramalho *et al.* 2017; Spieker *et al.* 2018). This process has been suggested to also occur in other oceanic volcano islands, such as the Cape Verde Islands (e.g. Lodge & Helffrich 2006; Ramalho *et al.* 2010a, b; Madeira *et al.* 2010), the Canaries (Lodge *et al.* 2012) and others (e.g. Gupta *et al.* 2010; Leahy *et al.* 2010; Fontaine *et al.* 2015). Yet, underplating does not seem to be an ubiquitous process associated with hotspots, since several oceanic islands located close to ridges do not exhibit it, such as Iceland and Ascension Island (e.g. Staples *et al.* 1997; Evangelidis *et al.* 2004). Spieker *et al.* (2018) interpreted a ∼7-km-thick layer in the lower crust at depths of ∼10–17 km in their models as evidence of magmatic underplating. We tested the sensitivity of our RWE data to such underplated layer by

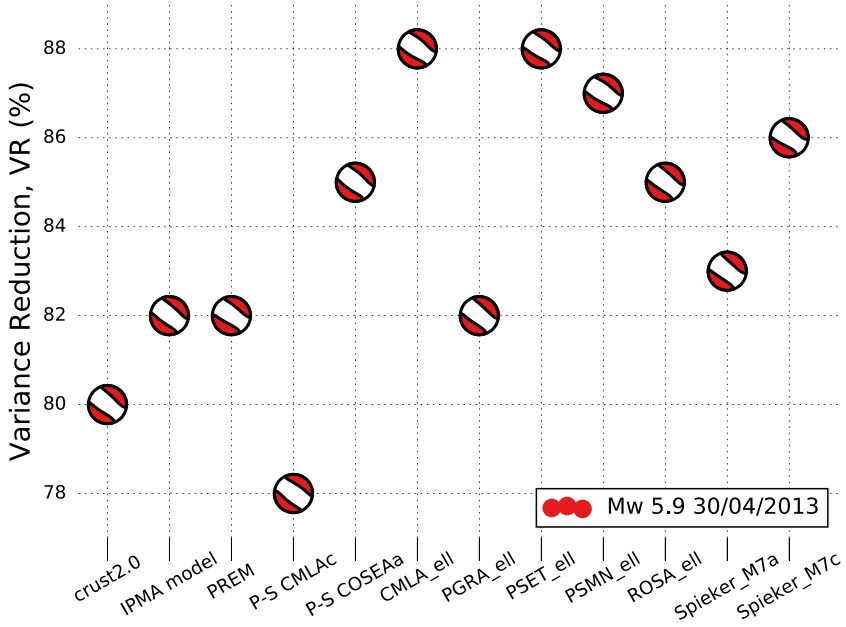

Figure 11. Comparison of the variance reduction and beachballs obtained from moment tensor inversions of local seismic data in the Azores for the various 1-D earth models considered: CRUST1.0 (Bassin *et al.* 2000); IPMA (adapted from Hirn *et al.* 1980); PREM (Dziewoński & Anderson 1981); P-S CMLAc, PS-COSEAa from Silveira *et al.* (2010); CMLA_ell, PGRA_ell, PSET_ell, PSMN_ell and ROSA_ell determined in this study; Spieker_M7a and Spieker_M7c from Spieker *et al.* (2018). Table S4 in the Supporting Information lists the parameters obtained in all the source inversions.

calculating the predicted RWE for 1-D V_S models with and without it. Fig. S8 in the Supporting Information shows that the presence of the underplated layer has a small effect on the RWE curve, only flattening it very slightly. The differences between the predicted RWE curves with and without underplating seem to be smaller than typical errors in RWE data (e.g. Fig. 6). Hence, it may be difficult to detect underplated layers with RWE measurements alone. In order to further test this, we performed inversions of RWE data from stations ROSA and CMLA using the same layer parametrization as in models Spieker-M7c and Spieker-M7a, respectively, that is, imposing the presence of underplated layers. Fig. S9 in the Supporting Information shows that this led to unstable inversions (e.g. for station ROSA) and/or to unrealistic model features (e.g. unlikely oscillations in V_S as a function of depth for both CMLA and ROSA, notably negative changes in V_S from crust to mantle across the Moho). Thus, teleseismic RWE data are not able to resolve thin underplated layers in the lower crust such as those reported by Spieker *et al.* (2018). On the other hand, the low V_S values obtained for station PSMN in Santa Maria compared to the other stations suggest that underplating due to magmatic intrusions may be possible beneath this island.

5.4 Outlook

In this study, we obtained median RWE by averaging the measurements for many earthquakes with a good azimuthal distribution. By computing full wave sensitivity kernels, Bao & Shen (2018) showed that RWE can resolve lateral structure in addition to that in the radial direction up to a distance of a wavelength from the receiver. On the one hand, this is a compelling prediction as it means that RWE can be inverted for 3-D structure in a volume tightly bound around the receiver. On the other hand, sensitivity to lateral structure can complicate the interpretation of 1-D depth inversions, which was also highlighted by Maupin (2017). Additionally, finite frequency effects can also affect measured RWEs. For instance, long-period ($T \sim 150$ s) teleseismic RWE measured by Ferreira & Woodhouse (2007b) deviated from expected values, which they interpreted as being due to finite frequency effects associated with small-scale heterogeneity in the mantle. Inverting multiperiod RWE for structure as we have done here can mitigate undesirable effects stemming from lateral sensitivity and finite frequency effects. Furthermore, future joint inversions of different types of data (e.g. RWE, receiver functions, surface wave dispersion) in the Azores can further minimize these potential issues.

Our independent moment tensor inversions of local waveforms using the new V_S models obtained in this study showed that they lead to stable moment tensor solutions. Compared to other 1-D earth models available for the study region, our V_S profiles produced some of the best data fits to the local data. Hence, the new 1-D V_S models should help better constrain seismic moment tensor solutions and the local seismicity of the Azores region. More generally, our study highlights the potential of Rayleigh wave ellipticity analyses to investigate the crustal structure of oceanic island volcanoes. Future events in the region may help to further validate our results, notably local events to the northwest of the archipelago, which may yield better fits of data from stations ROSA and PGRA.

The current paucity of stations precludes a more detailed analysis of the subsurface structure and geodynamic processes active in the Azores Archipelago. In particular, the lack of seismic stations in the westernmost islands of the archipelago—Flores and Corvo—limits our understanding of the evolution of the region as a whole. This can be overcome if a denser seismic network is installed covering other regions of the archipelago, notably by deploying ocean bottom seismometers around the islands. Long-term deployment of such networks will ensure the necessary density of data required to conduct future higher resolution imaging studies.

6 CONCLUSIONS

In this study we inverted teleseismic RWE measurements for 1-D V_S structure beneath five seismic stations located in the Azores Archipelago. RWE analyses are particularly suitable for oceanic islands such as the Azores because they are a single station, local observable and hence are not affected by uneven station distribution nor by along-path averaging and smearing effects that affect tomography studies. We tested the reliability of our 1-D crustal models by using them in moment tensor inversions of independent local seismic data. Compared to other existing crustal models of the region, we found that our models led to some of the best data fits, suggesting that they capture fine-scale crustal structure well. The shallow V_S structure in our new models (top ∼5 km), which is likely within the volcanic edifice (Spieker *et al.* 2018), is slower than in previous crustal models of the region. This has potential implications for future seismic hazard assessment, notably for ground motion predictions in the Azores Archipelago.

We find that the Moho depth beneath the westernmost islands considered in this study (São Jorge and Graciosa) is shallower (∼10 km) than beneath the Terceira, São Miguel and Santa Maria Islands (∼13–16 km) in the eastern part of the archipelago. Thus, the Moho depth appears to increase away from the Mid-Atlantic ridge as expected. However, the rate at which Moho depth increases seems to be higher than that predicted from a half-space plate cooling model, suggesting that local perturbations such as magmatic activity have modified lithospheric structure.

The V_S models appear to be positively correlated with the age of the islands (oldest volcanoes exhibiting fastest V_S) except for Santa Maria, the oldest island in the archipelago. The reduction in V_S of the easternmost islands also agrees well with substantial ongoing magmatic intrusions suggested to be driving uplift of that part of the archipelago. The relatively lower crustal V_S that we observe beneath Santa Maria, despite it being the oldest island, supports previous suggestions of underplating (Ramalho *et al.* 2017; Spieker *et al.* 2018). On the other hand, we did not find compelling evidence of underplating beneath other islands, but this may be due to the limited sensitivity of RWE to thin layers in the lower crust. Future joint inversions of different types of data (e.g. RWE, receiver functions, surface wave dispersion) from denser seismic deployments in the region will help refine our models.

ACKNOWLEDGEMENTS

This research was supported by NERC project NE/N011791/1 and by FCT project AQUAREL (PTDC/CTE-GIC/116819/2010). A.M.G.F. also thanks discussions supported by COST Action ES1401-TIDES. We gratefully acknowledge Dina Vales and Fernando Carrilho for providing us with the PM data from IPMA and for fruitful discussions. We are also grateful to the availability of global seismograms from the IRIS Data Services and the II, IU, GEOSCOPE and GEOFON networks. The seismic inversions presented in this study were carried out at UCL's computer clusters Legion and Grace. We thank Graça Silveira, Kathrin Spieker and Stéphane Rondenay for useful discussions and for kindly providing their 1-D models of the Azores. We are grateful to Ricardo Ramalho for his careful and thoughtful review of the paper. We thank two anonymous reviewers and editor Lapo Boschi for their useful comments, which helped improve this paper.

REFERENCES

Attanayake, J., Ferreira, A.M.G., Berbellini, A. & Morelli, A., 2017. Crustal structure beneath Portugal from teleseismic Rayleigh wave ellipticity, *Tectonophysics,* **712–713,** 344–361.

Azevedo, J. & Portugal Ferreira, M.R., 2006. The volcanotectonic evolution of Flores Island, Azores (Portugal), *J. Volc. Geotherm. Res.,* **156**(1–2), 90–102.

Bao, X. & Shen, Y., 2018. Full-waveform sensitivity kernels of component-differential travel times and ZH amplitude ratios for velocity and density tomography, *J. geophys. Res.,* **123,** 4829–4840.

Bassin, C., Laske, G. & Masters, G., 2000. The current limits of resolution for surface wave tomography in North America, *EOS, Trans. Am. Geophys. Un.,* **81** (48) F897 .

Becker, J.J. *et al.*, 2009. Global bathymetry and elevation data at 30 arc seconds resolution: SRTM30_PLUS, *Mar. Geod.,* **32**(4), 355–371.

Berbellini, A., Morelli, A. & Ferreira, A.M.G., 2017. Crustal structure of northern Italy from the ellipticity of Rayleigh waves, *Phys. Earth planet. Inter.,* **267,** 1–14.

Berbellini, A., Schimmel, M., Ferreira, A.M.G. & Morelli, A., 2019. Constraining S-wave velocity using Rayleigh wave ellipticity from polarization analysis of seismic noise, *Geophys. J. Int.,* **216,** 1817–1830.

Borges, J., Bezzeghoud, M., Buforn, E., Pro, C. & Fitas, A., 2007. The 1980, 1997 and 1998 Azores earthquakes and some seismo-tectonic implications, *Tectonophysics,* **435**(1–4), 37–54.

Bouchon, M., 1981. A simple method to calculate Green's functions for elastic layered media, *Bull. seism. Soc. Am.,* **71**(4), 959–971.

Brocher, T., 2005. Empirical relations between elastic wavespeeds and density in the earth's crust, *Bull. seism. Soc. Am.,* (95), 2081–2092.

Calvert, A., Moore, R., McGeehin, J. & da Silva, A., 2006. Volcanic history and 40Ar/39Ar and 14C geochronology of Terceira island, Azores, Portugal, *J. Volc. Geotherm. Res.,* **1–2**(156), 103–115.

Caress, D., McNutt, M., Detrick, R. & Mutter, J., 1995. Seismic imaging of hotspot-related crustal underplating beneath the Marquesas Islands, *Nature,* **373,** 600–603.

Chovelon, P., 1982, Evolution volcano-tectonique des îles de Faial et Pico, *PhD thesis,* Université Paris Sud 11.

Detrick, R.S., Needham, H.D. & Renard, V., 1995. Gravity anomalies and crustal thickness variations along the Mid-Atlantic Ridge between 33°N and 40°N, *J. geophys. Res.,* **100**(B3), 3767–3787.

Dias, N.A., Matias, L., Lourenço, N., Madeira, J., Carrilho, F. & Gaspar, J.L., 2007. Crustal seismic velocity structure near Faial and Pico Islands (AZORES), from local earthquake tomography, *Tectonophysics,* **445**(3–4), 301–317.

Dziewoński, A.M. & Anderson, D.L., 1981. Preliminary reference Earth model, *Phys. Earth planet. Inter.,* **25**(4), 297–356.

Escartín, J., Cannat, M., Pouliquen, G., Rabain, A. & Lin, J., 2001. Crustal thickness of v-shaped ridges south of the Azores: interaction of the Mid-Atlantic Ridge (36°-39°N) and the Azores hot spot, *J. geophys. Res.,* **106**(B10), 21 719–21 735.

Evangelidis, C., Minshull, T. & Henstock, T., 2004. Three-dimensional crustal structure of Ascension island from active source seismic tomography, *Geophys. J. Int.,* **159**(1), 311–325.

Ferreira, A.M.G. & Woodhouse, J.H., 2007a. Source, path and receiver effects on seismic surface waves, *Geophys. J. Int.,* **168**(1), 109–132.

Ferreira, A.M.G. & Woodhouse, J.H., 2007b. Observations of long period Rayleigh wave ellipticity, *Geophys. J. Int.,* **169,** 161–169.

Fontaine, F., Barruol, G., Tkalcic, H., Wölbern, I., Rümpker, G., Bodin, T. & Haugmard, M., 2015. Crustal and uppermost mantle structure variation beneath la Réunion hotspot track, *Geophys. J. Int.,* **203**(1), 107–126.

França, Z., Lago, M., Nunes, J.C., Galé, C., Forjaz, V.H., Ó, P. & Arranz, E., 2003. Geochemistry of alkaline basalts of Corvo Island (Azores, Portugal): preliminary data, *Geogaceta,* **40,** 87–90.

Frietsch, M., Ferreira, A., Vales, D. & Carrilho, F., 2018. On the robustness of seismic moment tensor inversions for mid-ocean earthquakes: the Azores Archipelago, *Geophys. J. Int.,* **215**(1), 564–584.

Gaspar, J.L., Queiroz, G., Ferreira, T., Medeiros, A.R., Goulart, C. & Medeiros, J., 2015. Chapter 4 Earthquakes and volcanic eruptions in

the Azores region: geodynamic implications from major historical events and instrumental seismicity, *Geol. Soc., Lond., Memoirs,* **44**(1), 33–49.

Gente, P., Dyment, J., Maia, M. & Goslin, J., 2003. Interaction between the Mid-Atlantic Ridge and the Azores hot spot during the last 85 Myr: emplacement and rifting of the hot spot-derived plateaus, *Geochem. Geophys. Geosyst.,* **4**(10), doi:10.1029/2003GC000527.

Gilbert, F., 1971. Excitation of the normal modes of the earth by earthquake sources, *Geophys. J. Int.,* **22**(2), 223–226.

Gupta, A., Mishra, A. & Rai, S.S., 2010. Magmatic underplating of crust beneath the Laccadive island, NW Indian ocean, *Geophys. J. Int.,* **183,** 536–542.

Herrmann, R., 2013. Computer programs in seismology: an evolving tool for instruction and research, *Seismol. Res. Lett.,* **84,** 1081–1088.

Hildenbrand, A., Madureira, P., Marques, F.O., Cruz, I., Henry, B. & Silva, P., 2008. Multi-stage evolution of a sub-aerial volcanic ridge over the last 1.3 Myr: S. Jorge island, Azores triple junction, *Earth planet. Sci. Lett.,* **273**(3–4), 289–298.

Hildenbrand, A., Marques, F.O., Costa, A.C.G., Sibrant, A.L.R., Silva, P.F., Henry, B., Miranda, J.M. & Madureira, P., 2012. Reconstructing the architectural evolution of volcanic islands from combined K/Ar, morphologic, tectonic, and magnetic data: the Faial island example (Azores), *J. Volc. Geotherm. Res.,* **241,** 39–48.

Hirn, A., Haessler, H., Trong, P.H., Wittlinger, G. & Victor, L.A.M., 1980. Aftershock sequence of the January 1st, 1980, earthquake and present-day tectonics in the Azores, *Geophys. Res. Lett.,* **7**(7), 501–504.

Hobiger, M. *et al.*, 2013. Ground structure imaging by inversions of Rayleigh wave ellipticity: sensitivity analysis and application to European strong-motion sites, *Geophys. J. Int.,* **192**(1), 207–229.

IPMA, 2016. *IPMA Instrumental Earthquake Database (1970–2016),* Instituto Português do Mar e da Atmosfera, Lisbon, Portugal.

Johnson, C.L., Wijbrans, J.R., Constable, C.G., Gee, J., Staudigel, H. & Tauxe, L., 1998. 40Ar/39Ar ages and paleomagnetism of São Miguel lavas, Azores, *Earth planet. Sci. Lett.,* **3–4**(160), 637–649.

Kendrick, J.E., Smith, R., Sammonds, P., Meredith, P.G., Dainty, M. & Pallister, P.D., 2013. The influence of thermal and cyclic stressing on the strength of rock from Mount St. Helens, Washington, *Bull. Volcanol.,* **75,** 1–12.

Larrea, P., Wijbrans, J.R., Galé, C., Ubide, T., Lago, M., França, Z. & Widom, E., 2014. $^{40}Ar/^{39}Ar$ constraints on the temporal evolution of Graciosa island, Azores (Portugal), *Bull. Volcanol.,* **76,** 796.

Leahy, G.M., Collins, J.A., Wolfe, C.J., Laske, G. & Solomon, S.C., 2010. Underplating of the Hawaiian swell: evidence from teleseismic receiver functions, *Geophys. J. Int.,* **183,** 313–329.

Lin, F.-C., Schmandt, B. & Tsai, V.C., 2012. Joint inversion of Rayleigh wave phase velocity and ellipticity using USArray: constraining velocity and density structure in the upper crust, *Geophys. Res. Lett.,* **39,** L12303.

Loaiza, S., Fortin, J., Schubnel, A., Gueguen, Y., Vinciguerra, S. & Moreira, M., 2012. Mechanical behavior and localized failure modes in a porous basalt from the Azores, *Geophys. Res. Lett.,* **39** (19), doi:10.1029/2012GL053218.

Lodge, A. & Helffrich, G., 2006. Depleted swell root beneath the Cape Verde islands, *Geology,* **34**(6), 449–452.

Lodge, A., Nippress, S.E.J., Rietbrock, A., García-Yeguas, A. & Ibanẽz, J.M., 2012. Evidence for magmatic underplating and partial melt beneath the Canary islands derived using teleseismic receiver functions, *Phys. Earth planet. Inter.,* **212,** 44–54.

Luis, J.F. & Neves, M.C., 2006. The isostatic compensation of the Azores plateau: a 3D admittance and coherence analysis, *J. Volc. Geotherm. Res.,* **156**(1–2), 10–22.

Madeira, J., Mata, J., Mourão, C., Brum da Silveira, A., Martins, S., Ramalho, R. & Hoffmann, D., 2010. Volcano-stratigraphic and structural evolution of Brava island (cape verde) from 40Ar/39Ar, U/Th and field constraints, *J. Volc. Geotherm. Res.,* **196,** 219–235.

Marques, F., Hildenbrand, A. & Hübscher, C., 2018. Evolution of a volcanic island on the shoulder of an oceanic rift and geodynamic implications: S. Jorge island on the Terceira Rift, Azores triple junction, *Tectonophysics,* **738–739,** 41–50.

Maupin, V., 2017. 3-D sensitivity kernels of the Rayleigh wave ellipticity, *Geophys. J. Int.,* **211,** 107–119.

McKenzie, D., Jackson, J. & Priestley, K., 2005. Thermal structure of oceanic and continental lithosphere, *Earth planet. Sci. Lett.,* **233**(3), 337–349.

McNutt, M. & Caress, D.W., 2007. Crust and lithospheric structure - hot spots and hot-spot swells, in *Treatise on Geophysics,* Vol. 3, pp. 453–478, doi:10.1016/B978-0-444-53802-4.00212-8.

Métrich, N., Zanon, V., Créon, L., Hildenbrand, A., Moreira, M. & Marques, F.O., 2014. Is the 'Azores hotspot' a wetspot? Insights from the geochemistry of fluid and melt inclusions in olivine of Pico basalts, *J. Petrol.,* **55**(2), 377–393.

Miranda, J.M., Luis, J.F., Lourenço, N. & Goslin, J., 2014. Distributed deformation close to the Azores triple point, *Mar. Geol.,* **355,** 27–35.

Müller, R.D., Sdrolias, M., Gaina, C. & Roest, W.R., 2008. Age, spreading rates, and spreading asymmetry of the world's ocean crust, *Geochem., Geophys., Geosyst.,* **9,** Q04006.

Mutter, C.Z. & Mutter, J.C., 1993. Variations in thickness of layer 3 dominate oceanic crustal structure, *Earth planet. Sci. Lett.,* **117,** 295–317.

Olsen, K.B., 2000. Site amplification in the Los Angeles basin from three-dimensional modeling of ground motion, *Bull. seism. Soc. Am.,* **6B**(90), S77–S94.

Parsons, B. & Sclater, J.G., 1977. An analysis of the variation of ocean floor bathymetry and heat flow with age, *J. geophys. Res.,* **82**(5), 803–827.

Pasyanos, M.E., Masters, T.G., Laske, G. & Ma, Z., 2014. Litho1.0: an updated crust and lithospheric model of the earth, *J. geophys. Res.,* **119,** 2153–2173.

Ramalho, R. *et al.*, 2017. Emergence and evolution of Santa Maria Island (Azores) - the conundrum of uplifted islands revisited, *Bull. Geol. Soc. Am.,* **129,** 372–390.

Ramalho, R., Helffrich, G., Cosca, M., Vance, D., Hoffmann, D. & Schmidt, D., 2010a. Episodic swell growth inferred from variable uplift of the Cape Verde hot spot islands, *Nat. Geosci.,* **3,** 774–777.

Ramalho, R., Helffrich, G., Cosca, M., Vance, D., Hoffmann, D. & Schmidt, D., 2010b. Vertical movements of ocean island volcanoes: insights from a stationary plate, *Mar. Geol.,* **275,** 84–95.

Rondenay, S., 2009. Upper mantle imaging with array recordings of converted and scattered teleseismic waves, *Surv. Geophys.,* **30,** 377–405.

Rychert, C.A. & Harmon, N., 2018. Predictions and observations for the oceanic lithosphere from S-to-P receiver functions and SS precursors, *Geophys. Res. Lett.,* **45,** 5398–5406.

Sambridge, M., 1999. Geophysical inversion with a neighbourhood algorithm - I searching a parameter space, *Geophys. J. Int.,* **138,** 479–494.

Schilling, J.-G., 1975. Azores mantle blob: rare-earth evidence, *Earth planet. Sci. Lett.,* **25**(2), 103–115.

Searle, R.C., 1976. Lithospheric structure of the Azores Plateau from Rayleigh-wave dispersion, *Geophys. J. Int.,* **44**(3), 537–546.

Shapiro, N.M., Campillo, M., Stehly, L. & Ritzwoller, M.H., 2005. High-resolution surface-wave tomography from ambient seismic noise, *Science,* **5715**(307), 1615–1618.

Shen, W. & Ritzwoller, M.H., 2016. Crustal and uppermost mantle structure beneath the United States, *Journal of Geophysical Research: Solid Earth,* **121**(6), 4306–4342.

Sibrant, A.L.R. *et al.*, 2015. Morpho-structural evolution of a volcanic island developed inside an active oceanic rift: S. Miguel island (Terceira rift, Azores), *J. Volc. Geotherm. Res.,* **301,** 90–106.

Silveira, D., Gaspar, J.L., Ferreira, T. & Queiroz, G., 2003. Reassessment of the historical seismic activity with major impact on S. Miguel Island (Azores), *Nat. Hazards Earth Syst. Sci.,* **3**(6), 615–623.

Silveira, G., Stutzmann, E., Davaille, A., Montagner, J.-P., Mendes-Victor, L. & Sebai, A., 2006. Azores hotspot signature in the upper mantle, *J. Volc. Geotherm. Res.,* **156**(1–2), 23–34.

Silveira, G., Vinnik, L., Stutzmann, E., Farra, V., Kiselev, S. & Morais, I., 2010. Stratification of the earth beneath the Azores from P and S receiver functions, *Earth planet. Sci. Lett.,* **299**(1–2), 91–103.

Sokos, E. & Zahradník, J., 2013. Evaluating centroid-moment-tensor uncertainty in the new version of ISOLA software, *Seismol. Res. Lett.,* **84**(4), 656–665.

Sokos, E.N. & Zahradník, J., 2008. ISOLA a Fortran code and a Matlab GUI to perform multiple-point source inversion of seismic data, *Comput. Geosci.,* **34**(8), 967–977.

Spieker, K., Rondenay, S., Ramalho, R., Thomas, C. & Helffrich, G., 2018. Constraints on the structure of the crust and lithosphere beneath the Azores islands from teleseismic receiver functions, *Geophys. J. Int.,* **213**(2), 824–835.

Staples, R.K., White, R.S., Brandsdóttir, B., Menke, W., Maguire, P.K. & McBride, J.H., 1997. Färoe-Iceland ridge experiment 1. Crustal structure of northeastern Iceland, *J. geophys. Res.,* **102**(B4), 7849–7866.

Stein, C.A. & Stein, S., 1992. A model for the global variation in oceanic depth and heat flow with lithospheric age, *Nature,* **6391**(359), 123–129.

Tanimoto, T. & Alvizuri, C., 2006. Inversion of the Hz ratio of microseisms for *S*-wave velocity in the crust, *Geophys. J. Int.,* **165,** 323–335.

Tanimoto, T. & Rivera, L., 2008. The ZH ratio method for long period seismic data: sensitivity kernels and observational techniques, *Geophys. J. Int.,* **172,** 187–198.

Thurber, C.H., 1993. Local earthquake tomography: velocities and Vp/Vs-theory, in *Seismic Tomography: Theory and Practice,* Chap. 20, pp. 563–583, eds Iyer, H.M. & Hirahara, K., Chapman and Hall.

USGS, 2017. *USGS Earthquakes Eventpage*.

Weiß, B., Hübscher, C. & Lüdmann, T., 2015. The tectonic evolution of the Southeastern Terceira Rift/São Miguel region (Azores), *Tectonophysics,* **654,** 75–95.

Weston, J., Ferreira, A.M.G. & Funning, G.J., 2011. Global compilation of interferometric synthetic aperture radar earthquake source models: 1. Comparisons with seismic catalogs, *J. geophys. Res.,* **116**(8), doi:10.1029/2010JB008131.

Weston, J., Ferreira, A.M.G. & Funning, G.J., 2012. Systematic comparisons of earthquake source models determined using InSAR and seismic data, *Tectonophysics,* **532–535,** 61–81.

Zanon, V., 2015. Chapter 5 The magmatism of the Azores islands, *Geol. Soc., Lond., Memoirs,* **44**(1), 51–64.

SUPPORTING INFORMATION

Supplementary data are available at *GJI* online.

Table S1. List of earthquakes used in this study (continued).

Table S2. Range of V_S values in km s^{-1} searched within each crustal layer for each station considered in this study and corresponding layer depth in kilometres. For stations ROSA and PGRA only three crustal layers are considered.

Table S3. Best-fitting V_S models obtained in this study from the inversion of Rayleigh wave ellipticity data along with the uncertainty in V_S (σ). The density ρ and compressional wave speed V_P are obtained from the Brocher relations (Brocher 2005).

Table S4. Source parameters from moment tensor inversions for the Povoação earthquake for all the sixteen 1-D crustal models considered in this study (see the main text for details). The solutions for the two fault planes determined in the inversions are shown. VR is the variance reduction, CTime is the time difference to IPMA's hypocentre, Lat, Lon, Depth are from IPMA's catalogue; DC is the double-couple component.

Figure S1. Geographical distribution of the optimal Moho depths determined in this study for the stations considered. The data from the westernmost seismic stations used in this study require a shallower Moho depth (∼10 km) than data from stations in the eastern part of the archipelago (∼13–16 km).

Figure S2. Scatter plots and distributions of all the V_S parameters in the three layers used in the RWE inversions for station PGRA. The best-fitting solution is marked by green crosses and vertical green lines. The parameters that correspond to solutions within 20 per cent of the best-fitting model are shown in black; all the other model parameters shown are in grey. Trade-offs between parameters would appear as diagonal features in the scatter plots.

Figure S3. Same as Fig. S2 but for station ROSA.

Figure S4. Same as Fig. S2 but for station PSET.

Figure S5. Same as Fig. S2 but for station PSMN.

Figure S6. Left-hand panel: evolution of inversion for station CMLA when inverting only for V_S in each crustal layer. Right-hand panel: evolution of inversion for station CMLA when inverting simultaneously for V_S in each crustal layer and for Moho depth.

Figure S7. Left-hand panel: results from the inversion of our RWE measurements for the joint determination of V_S and Moho depth for station CMLA. The profile in green corresponds to the formally best-fitting model. The models in black lead to data misfit values within 20 per cent of the best-fitting model. The models in grey are all the models sampled in the inversion process. The minimum misfit Moho depth is annotated. Right-hand panel: comparison between our RWE observations (blue dots with error bars) and predictions for the best-fitting model shown on the left. The predicted RWE curves for the models within 20 per cent of the best-fitting models are also shown (black curves) as well as for all the models sampled in the inversion process (grey lines).

Figure S8. Theoretical predictions of Rayleigh wave ellipticity (right) for a 1-D V_S model with an underplated layer (blue profile, left-hand panel) and without an underplated layer (orange profile, left-hand panel). The 1-D profile with an underplated layer (blue) corresponds to the model M7c of Spieker *et al*. (2018).

Figure S9. Same as in Fig. 5 of the main manuscript for station CMLA but using the layered parametrization from model M7a of Spieker *et al*. (2018) in the RWE data inversions (left-hand panel) and for station ROSA using the layered parametrization from model M7c of Spieker *et al*. (2018) (right-hand panel). For reference, models M7a (left-hand panel) and M7c (right-hand panel) of Spieker *et al*. (2018) are shown in red.

Please note: Oxford University Press is not responsible for the content or functionality of any supporting materials supplied by the authors. Any queries (other than missing material) should be directed to the corresponding author for the paper.